nature geoscience

Article

https://doi.org/10.1038/s41561-025-01653-z

Evidence for pre-Noachian granitic rocks on Mars from quartz in meteorite NWA 7533

Received: 21 February 2024

Accepted: 27 January 2025

Published online: 21 February 2025

Check for updates

V. Malarewicz[1,2], O. Beyssac[1] ✉, B. Zanda[1,3], J. Marin-Carbonne[4], H. Leroux[5], D. Rubatto[4,6], A. S. Bouvier[4], D. Deldicque[7], S. Pont[1], S. Bernard[1], E. Bloch[8], S. Bouley[2], M. Humayun[9] & R. H. Hewins[1,10]

The surface of Mars has long been seen as a basaltic, monotonous world, but observations in the past decade have revealed more petrological diversity. Orbital and in situ rover investigations show that Mars developed a silica-rich crust early in its history. This is supported by studies of the Martian regolith breccia Northwest Africa (NWA) 7533 (and paired meteorites). When and to what extent rocks on Mars differentiated, and which geodynamical process could lead to this evolution, is still unclear. Here we use petrology and in situ geochemical analyses to document the presence of quartz in lithic clasts of NWA 7533. The clasts have a granitic composition with a mineral assemblage dominated by quartz, potassium feldspar and plagioclase. Such quartz-bearing clasts are the most evolved silicic rocks yet recognized among differentiated Martian lithologies. These clasts suggest the likely existence of pre-Noachian granitic rocks on Mars that formed in the presence of water. In bulk composition they resemble the oldest terrestrial rocks (Acasta gneisses, Canada) and also rocks from the large Sudbury impact structure. Therefore, we suggest that the combined action of hydrothermal activity and impact melting could have triggered the formation of granitic rocks and evolved crust on early Mars and Earth.

Quartz, the emblematic mineral of the Earth's continental crust, is rarely found in other planetary bodies. On Earth, quartz is an ultimate marker of magmatic differentiation of the continental crust, but it can also be locally crystallized by hydrothermal processes. Finding quartz and investigating the initial formation of continental crust in the primitive Hadean Earth (>4 Gyr ago; Ga) is challenging as plate tectonics perpetually recycles the crust, and the relevant rock record has largely vanished[1]. However, this early history may be traced on Mars because it experienced an early geodynamic evolution similar to that of the Earth without having subsequently developed plate tectonics[1]. Therefore, Mars preserves abundant pre-Noachian (>4.1 Ga) and Noachian (~4.1–3.7 Ga) rocks at its surface[1], including a thick crust in the southern highlands[2] as well as bodies of differentiated rocks[3] (Supplementary Note 1). Interestingly, in situ exploration of the Noachian terrains of Gale Crater by the Curiosity rover detected silica-rich float rocks with granodioritic compositions, including K-feldspar and 'translucent grey grains'[4] (evocative of quartz). Quartz-free, differentiated monzonitic and related lithic fragments occur in the Martian polymict breccia Northwest Africa (NWA) 7533 and in paired meteorites[5–8] with alkali compositions similar to those of Gale Crater rocks. Here we report

[1]Muséum National d'Histoire Naturelle, Sorbonne Université, UMR CNRS 7590, Institut de Minéralogie de Physique des Matériaux et de Cosmochimie, Paris, France. [2]Université Paris-Saclay, UMR CNRS 8148, GEOPS, Orsay, France. [3]Laboratoire Temps Espace, UMR CNRS 8255, Paris, France. [4]Institut de Sciences de la Terre, University of Lausanne, Lausanne, Switzerland. [5]Université de Lille, INRAE, Centrale Lille, UMR CNRS 8207-UMET-Unité Matériaux et Transformations, Lille, France. [6]Institute of Geological Sciences, University of Bern, Bern, Switzerland. [7]Laboratoire de Géologie, Département de Géosciences, École Normale Supérieure, UMR CNRS 8538, PSL University, Paris, France. [8]Lunar and Planetary Laboratory, University of Arizona, Tucson, AZ, USA. [9]Department of Earth, Ocean & Atmospheric Science and National High Magnetic Field Laboratory, Florida State University, Tallahassee, FL, USA. [10]Department of Earth & Planetary Sciences, Rutgers University, Piscataway, NJ, USA. ✉e-mail: Olivier.Beyssac@sorbonne-universite.fr

the discovery of multiple silica grains in a specific clast-laden melt rock (CLMR)[8] of NWA 7533. Some silica grains are contained within felsic igneous clasts and some are isolated in the melt matrix. We show that these grains are crystalline quartz and characterize their chemistry, isotopic composition, structure and microtexture down to the sub-micrometre scale. We then discuss the processes that may be involved in the formation of this quartz and present some implications for the earliest history of Mars and Earth.

Quartz in NWA 7533

NWA 7533 regolith breccia (and paired meteorites) contains a wide variety of clasts embedded in a fine-grained crystalline matrix of basaltic composition[5–9]. These clasts include CLMRs and spherules, plus crystal shards and igneous clasts, such as monzonitic and noritic clasts and fine-grained microbasaltic fragments, all interpreted as impact melt rocks[5,8]. The mineralogy of these clasts includes K-feldspar, plagioclase, pyroxene, chlorapatite and (Ti)–Fe oxides. Zircon has been found in clasts and as grains within the matrix, revealing complex crystallization processes that began ~4.48 Ga according to the U–Pb age of zircon in NWA 7533 and paired samples[5,9–11]. Petrological investigations of NWA 7533 (Fig. 1a and Extended Data Fig. 1) revealed a body with a dendritic groundmass (dendrites <10 µm in length) and a vitrophyric melt core (Extended Data Fig. 2) interpreted as a CLMR. The bulk composition of this CLMR is depleted in MgO and enriched in CaO compared with the breccia matrix and other CLMRs of the meteorite (Extended Data Fig. 3 and Supplementary Table 1). More than 130 SiO_2-rich grains of various shapes and sizes were detected in this CLMR (Fig. 1a and Supplementary Fig. 1). Electron microprobe analyses confirm that these grains have a pure SiO_2 composition (Supplementary Table 2), consistent with quartz.

Raman spectra of these SiO_2-rich grains are consistent with crystalline quartz (Fig. 2a). More than 40 of the largest silica grains (>20 µm) were analysed and show comparable spectra with a sharp peak at 464 cm^{-1} (involving O motion in Si–O–Si symmetric stretching–bending mode) and less intense peaks at 128, 206, 265 and 355 cm^{-1} (torsional vibrations and O–Si–O bending modes) consistent with crystalline quartz[12]. Raman hyperspectral mapping shows that the position and full width at half maximum of the 464 cm^{-1} peak are constant within the quartz grains, reflecting their homogeneous high crystallinity. We did not find the Raman features characteristic of SiO_2 glass, or of high-pressure or high-temperature SiO_2 polymorphs found in other Martian meteorites[13,14]. No important shift in position or broadening of the main peak at 464 cm^{-1} was detected within or between grains, suggesting at most a low density of shock-induced defects. Quartz crystals scattered throughout the melt zone vary from rounded to angular, sometimes compact or with a more irregular texture (Supplementary Fig. 1). Crystal length ranges from sub-micrometre to ~130 µm, mostly exceeding 10 µm in length. Most quartz grains are isolated in the melt matrix and are not euhedral as they are fragments of originally larger grains. A few large grains form lithic clasts with feldspar and pyroxene (Fig. 1b,c and Extended Data Fig. 4). The cathodoluminescence signal, caused by structural heterogeneities such as lattice defects[15], varies among the grains (Fig. 1e and Supplementary Fig. 1). Quartz grains in lithic clasts show a strong, homogeneous luminescence signal. Isolated grains in the melt matrix often have a zoned luminescence pattern indicating growth layers. In some isolated grains, the truncation of the luminescence patterns at the crystal edges (Fig. 1e) indicates that quartz grains crystallized and were fragmented prior to their incorporation into the CLMR.

Four ultrathin sections were extracted by focused ion beam (FIB) from representative quartz grains, isolated in the melt matrix or from lithic clasts, exhibiting diverse luminescence patterns (Extended Data Fig. 5). Transmission electron microscopy (TEM) imaging and electron diffraction show that all quartz grains are single crystals (Fig. 2b and Extended Data Fig. 5). Only minor structural defects and a few mineral inclusions, mostly sulfides and (Ti)–Fe oxides, were identified in one quartz grain (Extended Data Fig. 6). Two FIB sections contain thin planar defects (a few nanometres wide) in the form of dislocations oriented according to (0001), interpreted as mechanical twins (Fig. 2b and Extended Data Fig. 6), indicative of a low-intensity shock process[16]. The density of such planar defects is quite variable among and within the grains. In one sample (Extended Data Fig. 6c), we detected an amorphous lamella with an orientation close to $(10\bar{1}3)$. One sample contains thin planar defects parallel to $(10\bar{1}1)$ (Extended Data Fig. 6e). Planar defects in planes $(10\bar{1}3)$ observed are comparable to planar deformation features developed in quartz subjected to shock pressures of ~10 GPa (ref. 17).

Microtexture and geochemistry

Quartz-bearing clasts (QBC) display diverse mineral assemblages and microtextures (Fig. 1 and Extended Data Fig. 4). Some clasts are texturally similar to noritic–monzonitic clasts previously described in NWA 7533 (refs. 6–8), but with large quartz crystals as well as K-feldspar ($An_{0.8–2.7}Ab_{7.7–19.3}Or_{78.0–91.4}$) and plagioclase ($An_{0.8–65.9}Ab_{30.8–93.7}Or_{3.3–5.5}$), ± pyroxene ($En_{45.5}Fs_{46.2}Wo_{8.3}$), ± ilmenite ± chlorapatite (Supplementary Table 2 and Extended Data Fig. 7). One felsite clast (Fig. 1d) contains intergrowths of quartz and K-feldspar, with a microtexture similar to that of clasts in the lunar regolith breccia NWA 11962 (ref. 18). Other clasts (Extended Data Fig. 4b) resemble microgranites, with quartz finely intergrown with perthitic feldspar ($An_{0.8}Ab_{12.5}Or_{86.7}$–$An_{1.6}Ab_{88.2}Or_{10.2}$). Such microtextures of quartz and feldspar are common in terrestrial granitic plutonic rocks due to the simultaneous crystallization of quartz and feldspar[19]. Lastly, some clasts (Extended Data Fig. 4a) share a similar mineral assemblage and texture with the granitic clast described in the ordinary chondrite regolith breccia Adzhi-Bogdo[20].

Quartz $\delta^{18}O$ values show large variability ranging from +5 to +12 ‰, with most data clustered in the 8–12‰ range (Fig. 3a) for both isolated and QBC grains. This is higher than the bulk values of Martian shergottites, nakhlites and chassignites (SNC meteorites; 3.5–5.5‰) and NWA 7034 breccia (6.35 ± 0.5‰)[21], and the Earth's bulk mid-ocean ridge basalt (MORB) value (5.5 ± 0.5‰)[22]. Such $\delta^{18}O$ values are consistent with terrestrial granitic quartz, especially that older than 2 Gyr (ref. 23), but also with hydrothermal quartz[24]. Quartz $\delta^{30}Si$ values also show large variability, from around +0.5 to +6 ‰ (Fig. 3b), significantly higher than for hydrothermal, magmatic or Archaean sedimentary (chert) quartz on Earth[24–26] or bulk Martian SNC meteorites[27]. Such elevated $\delta^{18}O$ and $\delta^{30}Si$ values, and their variability, are best explained by the magma incorporating a component previously altered by low-temperature water–rock interactions and bearing clay minerals (Supplementary Note 2). Furthermore, the Ti content measured in quartz yields crystallization temperatures of ~650–880 °C in a pressure range of 2–10 kbar (ref. 28), within the present-day thickness range (30–72 km)[29] of the Martian crust (Extended Data Fig. 8).

The textures of the QBC, the structure of the quartz, and its O and Si isotopic and Ti compositions are consistent with a magmatic origin. The chemical compositions of the QBC plotted in geochemical classification diagrams (Fig. 4, Extended Data Fig. 9 and Supplementary Tables 3 and 4) show that the compositions of clasts 2, 3 and 5 are those of a granite. Clasts 1 and 4, including various oxides and pyroxene ($En_{45.3}Fs_{46.9}Wo_{7.8}$), are closer to quartz diorite and granodiorite. Clasts 2 and 3 could be related to the monzonitic clasts described by previous studies[6–9], and represent the most differentiated endmember of this crystallization sequence. QBC and their host CLMR most probably formed along with the other differentiated clasts of the breccia ~4.31–4.48 Ga. Unfortunately, no zircon has been found in them to confirm this. However, all zircon grains found in other differentiated clasts yielded U–Pb ages of 4.31–4.48 Gyr (refs. 5–11), while ^{146}Sm–^{142}Nd and ^{147}Sm–^{143}Nd ages for mineral separates from the bulk rock show that all breccia components formed ~4.44 Ga (ref. 30).

Quartz has not been formally characterized in situ on Mars, either by robotic or orbital exploration, although its presence may explain

https://doi.org/10.1038/s41561-025-01653-z

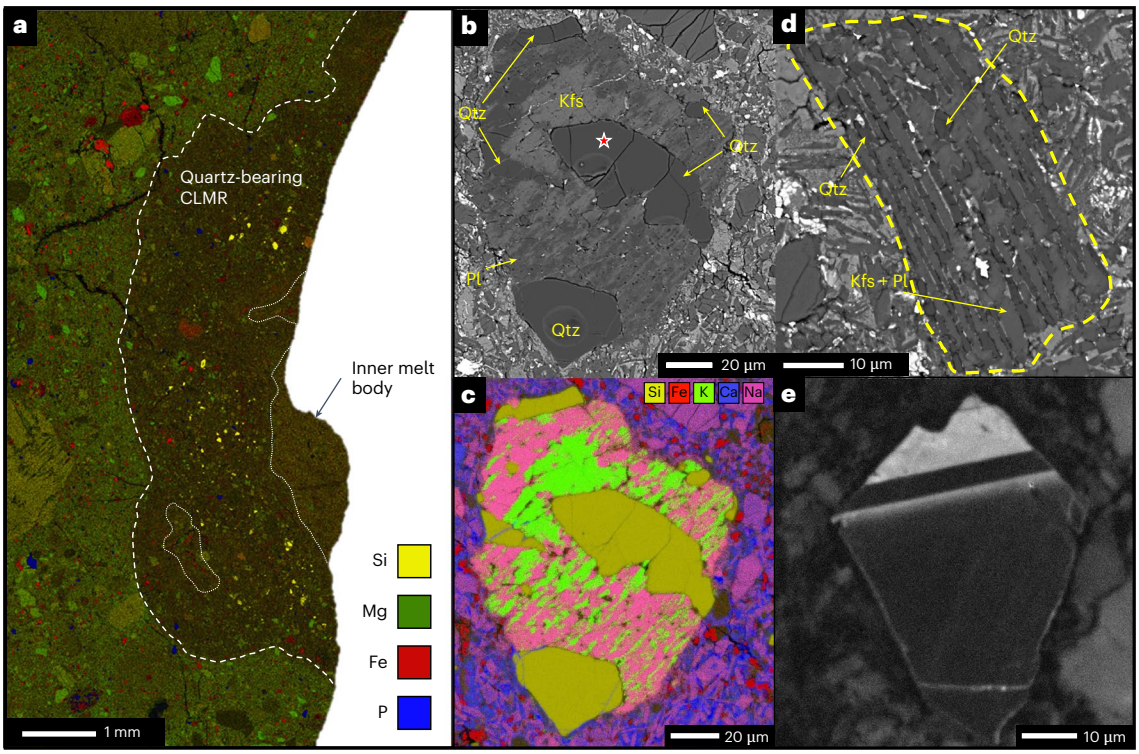

Fig. 1 | Quartz in NWA 7533. a, SEM EDS Si, Mg, Fe and P mapping of the quartz-bearing CLMR located in section SP10 of NWA 7533. This CLMR is depleted in Mg and enriched in Ca compared with the bulk surrounding matrix of the meteorite (Extended Data Fig. 3). An inner vitrophyric melt body is visible within the quartz-bearing CLMR (Extended Data Fig. 2), surrounded by a constellation of SiO_2-rich hotspots (yellow), identified as quartz fragments. **b**, SEM image illustrating quartz (Qtz) grains of varying size associated with K-feldspar (Kfs) and plagioclase (Pl) in a perthitic texture forming a lithic clast. The star indicates location for Raman spectrum in Qtz no. 1. **c**, SEM EDS Na, Ca, K, Fe and Si mapping of the clast shown in **b**. Note the fine textural mixing of K-feldspar and plagioclase. **d**, SEM image of another quartz-bearing clast (Qtz no. 5) composed of quartz lamellae finely intergrown with K-feldspar and plagioclase (see EDS mapping in Extended Data Fig. 4d). **e**, Cathodoluminescence image of Qtz no. 13 revealing the existence of a zonation, probably a growth pattern, interrupted abruptly at the quartz grain edges.

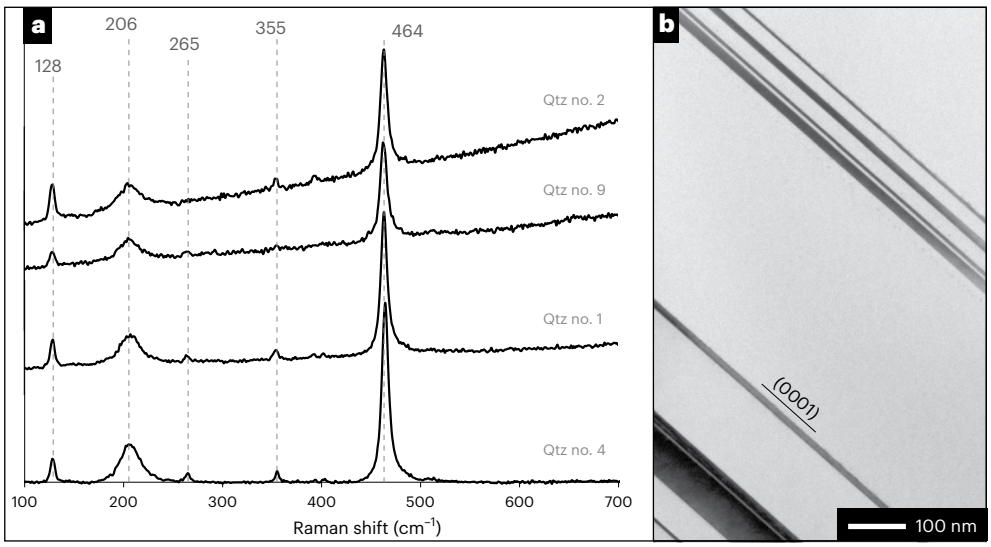

Fig. 2 | Quartz identification by Raman spectroscopy and TEM. a, Raman spectra from various SiO_2-rich grains found in the quartz-bearing CLMR, all identical and corresponding to crystalline quartz. **b**, Close-up TEM image of an FIB section from Qtz no. 13 in low-magnification bright-field mode showing planar defects in (0001) interpreted as mechanical twinning, illustrated by the alternation of intensity signal due to varying orientation of the crystal in the defect zone. See more TEM images in Extended Data Figs. 5 and 6.

some findings by Mars Science Laboratory Curiosity like CheMin X-ray diffractograms[31] or the observation of 'translucent grey grains' in felsic rocks[4], or visible–infrared reflectance spectral data from orbit (Supplementary Note 1). Two main occurrences of quartz in Martian meteorites are known before our discovery in NWA 7533. Quartz ± cristobalite occurs in small crystallization pockets interstitial to other phases in Nakhla[32] and shergottites[33,34]. These interstitial pockets contain K-feldspar and minor fayalitic olivine[33] but no plagioclase, ilmenite

https://doi.org/10.1038/s41561-025-01653-z

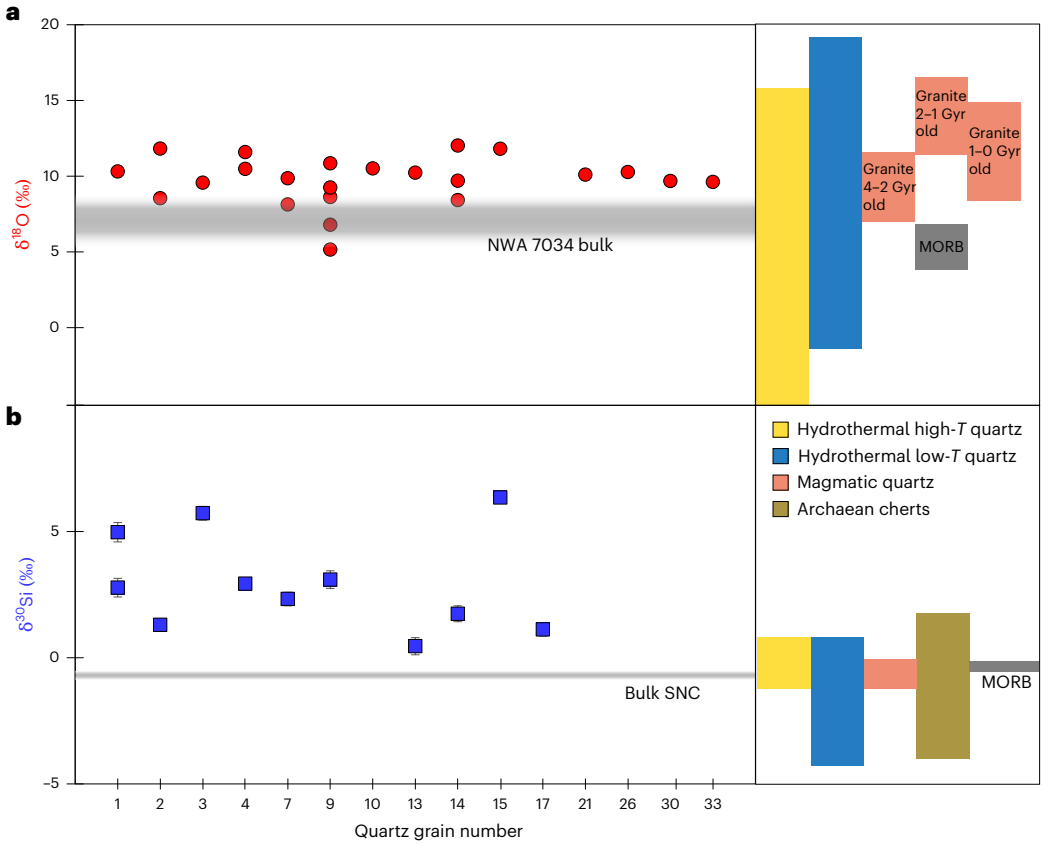

Fig. 3 | Quartz O and Si isotopic composition. a, $\delta^{18}O$ analyses from several quartz grains compared with the bulk breccia $\delta^{18}O$ value[21]. The right panel shows the range of $\delta^{18}O$ of quartz in relevant terrestrial settings: low and high hydrothermal quartz[24], magmatic quartz found in granite of various ages and MORB[22,23]. **b**, $\delta^{30}Si$ results from several quartz grains compared with the bulk value of SNC Martian meteorites[27]. The right panel shows the range of $\delta^{30}Si$ of quartz in relevant terrestrial settings: low-temperature and high-temperature hydrothermal quartz[24], magmatic quartz found in granite[25], quartz found in Archaean cherts[26] and MORB[24]. *T*, temperature. Note that error bars on isotopic measurements are mostly contained within the markers (see data and errors in Supplementary Tables 5 and 6).

or pyroxene as observed in the QBCs. These pockets are interpreted as late-stage crystallization products, due to a high degree of fractional crystallization of a basaltic magma. Different mineral assemblages and more diverse microtextures in QBCs probably reflect different magmatic processes for QBC formation. In the second case, quartz occurs with high-pressure SiO_2 polymorphs (for example, coesite) and SiO_2 glasses in shocked Martian meteorites[13,14]. Our investigations show that quartz occurs in NWA 7533 as a major phase in lithic clasts, and as single crystals with no high-pressure SiO_2 polymorphs, which rules out scenarios involving late-stage crystallization in local pockets and/or shock for its formation. This is also consistent with the absence of any other evidence for major shock in this meteorite.

Quartz formation by hydrothermalism and impact melting

From a broader perspective, orbital spectroscopy has reported that plagioclase is abundant in some regions of Mars as well as other differentiated lithologies[3] (Supplementary Note 1). Udry et al.[35] used models of fractional crystallization and terrestrial geochemical data to test formation scenarios for the evolved rocks at Gale Crater, and in meteorites including NWA 7533. They determined conditions that could produce monzonitic and granitic liquid compositions. They concluded that the Martian evolved rocks are more comparable to fractionated magmas produced in Earth's intraplate volcanoes than to terrestrial felsic magmas such as tonalite–trondhjemite–granodiorite (TTG) suites widespread in the Archaean Earth[36]. The finding of QBCs moderates this interpretation because their high bulk SiO_2 (>70%) is consistent with TTG composition, but rare in intraplate magmas (Fig. 4 and Extended Data Fig. 9). Nonetheless, the QBCs show FeO enrichment as well as lower Na_2O/K_2O ratio compared with TTGs (Extended Data Fig. 9). Comparing QBCs and the oldest rocks known on Earth may, however, still prove instructive. The oldest terrestrial minerals are the 4.0–4.2-Gyr-old (refs. 37–40) Jack Hills zircons, with a few grains going to ~4.3 Ga (ref. 39), yet these are detrital grains with no remnants of their initial host rock. However, these zircons have silica-rich mineral inclusions (for example, quartz, K-feldspars, plagioclase, phyllosilicates)[39] plus rare-earth element patterns[40,41] and Lu–Hf isotopes[42], suggesting crystallization in a TTG-like granitoid magma. In addition, Jack Hills zircons have supracrustal $\delta^{18}O$ values of 4.3–7.3‰ (refs. 37,38), suggesting the presence of liquid water very early in Earth history[39,40]. A similar conclusion was reached recently by the analysis of Hadean zircons in the Barberton Greenstone Belt in South Africa[43]. Calculation of the $\delta^{18}O$ value of zircon in equilibrium with our quartz grains at 700–800 °C (Extended Data Fig. 10) yields $\delta^{18}O$ values (~5–9‰), comparable to the values of the Jack Hills zircons, suggesting a similar process of incorporation of a recycled hydrous component in the parent magma[39].

The oldest terrestrial rocks are the ~4.02-Gyr-old Idiwhaa tonalitic gneisses of the Acasta Gneiss Complex (Canada). The Idiwhaa gneisses are characterized by FeO enrichment and high $Na_2O + K_2O$ compared with Archaean TTGs or Acasta felsic gneisses (<3.95 Gyr old)[44,45]. The composition of the QBCs is most similar to the Idiwhaa tonalitic gneisses, despite greater variability (Fig. 4 and Extended Data Fig. 9), suggesting similar formation processes. The Idiwhaa gneisses may have formed in an Iceland-like tectonic setting involving

https://doi.org/10.1038/s41561-025-01653-z

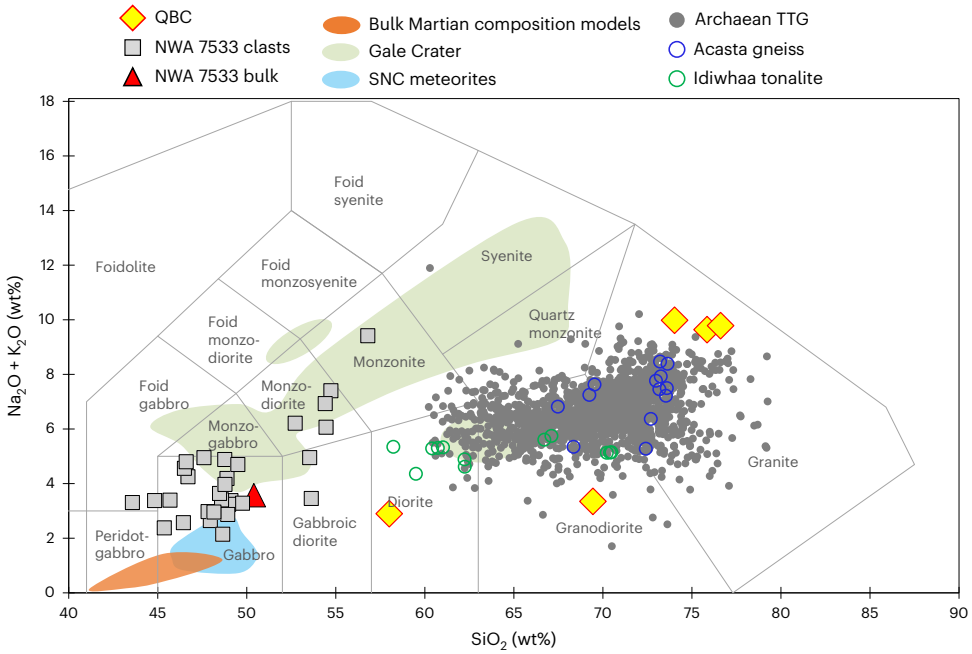

Fig. 4 | Geochemistry of QBC. $Na_2O + K_2O$ versus SiO_2 total alkali silica diagram depicting the QBC compared with the petrological diversity of the lithic clasts found within the breccia[6–8], other Martian meteorites (SNC)[35], differentiated rocks from Gale Crater[4], bulk Martian composition models[50] and terrestrial rocks like the Archaean TTGs[36], the Acasta gneiss and Idiwhaa tonalite[44]. See Methods, Extended Data Fig. 9 and Supplementary Table 3 for data and errors.

assimilation of hydrothermally altered rocks by a fractionating basaltic magma[45]. Alternatively, they may have formed by partially melting Fe-rich hydrated basaltic rocks (amphibolites) requiring considerable heat at shallow depth, best explained by impact melting[44]. The latter is a logical interpretation for the origin of Martian QBCs if the prevalence of large impact craters on the pre-Noachian surface of the planet is taken into account. All the paired breccia meteorites are essentially identical and represent a point source in a vast crater, yet we have evidence of a different horizon with 'granitic' material and a peculiar composition CLMR, implying diverse crustal remelting. Notably, the second-largest surviving terrestrial crater, Sudbury (Canada), has a thick melt sheet of granodioritic bulk composition comprising granophyre overlying norite[46,47] with compositions comparable to those of the noritic to granitic clasts in NWA 7533. We conclude that NWA 7533 collected at least two different rock types from various stratigraphic levels of the melt sheet. It has also been proposed that large impact basins formed on the Hadean Earth had (total) impact melt pools that differentiated and crystallized abundant felsic rocks[48]. The largest Martian impact basins would also generate partial melt zones at mantle depths, causing intrusion into the crust and formation of differentiated rocks[49].

In conclusion, the process that crystallized quartz in NWA 7533 requires the prior existence of an altered component. This implies strong interactions between the Martian hydrosphere and the planet's surface during the initial 100 Myr of its history. The QBCs and other clasts in NWA 7533 represent the most ancient fragments of a nascent Si-rich crust forming almost immediately after planetary accretion. The interplay between impact melting and hydrothermal activity played a key role in the formation of such crustal rocks on Mars, as in the Hadean Earth.

Online content

Any methods, additional references, Nature Portfolio reporting summaries, source data, extended data, supplementary information, acknowledgements, peer review information; details of author contributions and competing interests; and statements of data and code availability are available at https://doi.org/10.1038/s41561-025-01653-z.

References

1. Lapôtre, M. G. A. et al. Mars as a time machine to Precambrian Earth. *J. Geol. Soc.* **179**, jgs2022-047 (2022).
2. Bouley, S. et al. A thick crustal block revealed by reconstructions of early Mars highlands. *Nat. Geosci.* **13**, 105–109 (2020).
3. Phillips, M. S. et al. Extensive and ancient feldspathic crust detected across north Hellas rim, Mars: possible implications for primary crust formation. *Geology* **50**, 1182–1186 (2022).
4. Sautter, V. et al. In situ evidence for continental crust on early Mars. *Nat. Geosci.* **8**, 605–609 (2015).
5. Humayun, M. et al. Origin and age of the earliest Martian crust from meteorite NWA 7533. *Nature* **503**, 513–516 (2013).
6. Wittmann, A. et al. Petrography and composition of Martian regolith breccia meteorite Northwest Africa 7475. *Meteorit. Planet. Sci.* **50**, 326–352 (2015).
7. Santos, A. R. et al. Petrology of igneous clasts in Northwest Africa 7034: implications for the petrologic diversity of the Martian crust. *Geochim. Cosmochim. Acta* **157**, 56–85 (2015).
8. Hewins, R. H. et al. Regolith breccia Northwest Africa 7533: mineralogy and petrology with implications for early Mars. *Meteorit. Planet. Sci.* **52**, 89–124 (2017).
9. McCubbin, F. M. et al. Geologic history of Martian regolith breccia Northwest Africa 7034: evidence for hydrothermal activity and lithologic diversity in the Martian crust. *J. Geophys. Res.* **121**, 2120–2149 (2016).
10. Hu, S. et al. Ancient geologic events on Mars revealed by zircons and apatites from the Martian regolith breccia NWA 7034. *Meteorit. Planet. Sci.* **54**, 850–879 (2019).
11. Costa, M. M. et al. The internal structure and geodynamics of Mars inferred from a 4.2-Gyr zircon record. *Proc. Natl Acad. Sci. USA* **117**, 30973–30979 (2020).
12. Kingma, K. J. & Hemley, R. J. Raman spectroscopic study of microcrystalline silica. *Am. Mineral.* **79**, 269–273 (1994).
13. Aoudjehane, H. C., Jambon, A., Reynard, B. & Blanc, P. Silica as a shock index in shergottites: a cathodoluminescence study. *Meteorit. Planet. Sci.* **40**, 967–979 (2005).

14. Hewins, R. et al. Pervasive shock melting at >65 GPa in a Martian basalt, the shergottite Northwest Africa 14672. *Meteorit. Planet. Sci* **59**, 640–669 (2023).
15. Götze, J., Plötze, M. & Habermann, D. Origin, spectral characteristics and practical applications of the cathodoluminescence (CL) of quartz - a review. *Mineral. Petrol.* **71**, 225–250 (2001).
16. Leroux, H., Reimold, W. U. & Doukhan, J.-C. A TEM investigation of shock metamorphism in quartz from the Vredefort Dome, South Africa. *Tectonophysics* **230**, 223–239 (1994).
17. Stöffler, D. & Langenhorst, F. Shock metamorphism of quartz in nature and experiment: I. Basic observation and theory. *Meteoritics* **29**, 155–181 (1994).
18. Bechtold, A. et al. Lunar meteorite Northwest Africa 11962: a regolith breccia containing records of titanium-rich lunar volcanism and the high alkali suite. *Meteorit. Planet. Sci.* **56**, 971–991 (2021).
19. Xu, H. et al. Crystallographic evidence for simultaneous growth in graphic granite. *Gondwana Res.* **27**, 1550–1559 (2015).
20. Terada, K. & Bischoff, A. Asteroidal granite-like magmatism 4.53 gyr ago. *Astrophys. J.* **699**, L68 (2009).
21. Agee, C. B. et al. Unique meteorite from early Amazonian Mars: water-rich basaltic breccia Northwest Africa 7034. *Science* **339**, 780–785 (2013).
22. Mattey, D., Lowry, D. & Macpherson, C. Oxygen isotope composition of mantle peridotite. *Earth Planet. Sci. Lett.* **128**, 231–241 (1994).
23. Bindeman, I. N. Triple oxygen isotopes in evolving continental crust, granites, and clastic sediments. *Rev. Mineral. Geochem.* **86**, 241–290 (2021).
24. Kleine, B. I., Stefánsson, A., Halldórsson, S. A., Whitehouse, M. J. & Jónasson, K. Silicon and oxygen isotopes unravel quartz formation processes in the Icelandic crust. *Geochem. Perspect. Lett*. https://doi.org/10.7185/geochemlet.1811 (2018).
25. Savage, P. S., Georg, R. B., Williams, H. M. & Halliday, A. N. The silicon isotope composition of the upper continental crust. *Geochim. Cosmochim. Acta* **109**, 384–399 (2013).
26. Marin-Carbonne, J., Chaussidon, M. & Robert, F. Micrometer-scale chemical and isotopic criteria (O and Si) on the origin and history of Precambrian cherts: implications for paleo-temperature reconstructions. *Geochim. Cosmochim. Acta* **92**, 129–147 (2012).
27. Armytage, R. M. G., Georg, R. B., Savage, P. S., Williams, H. M. & Halliday, A. N. Silicon isotopes in meteorites and planetary core formation. *Geochim. Cosmochim. Acta* **75**, 3662–3676 (2011).
28. Huang, R. & Audétat, A. The titanium-in-quartz (TitaniQ) thermobarometer: a critical examination and re-calibration. *Geochim. Cosmochim. Acta* **84**, 75–89 (2012).
29. Wieczorek, M. A. et al. InSight constraints on the global character of the Martian crust. *J. Geophys. Res.* **127**, e2022JE007298 (2022).
30. Nyquist, L. et al. Rb–Sr and Sm–Nd isotopic and REE studies of igneous components in the bulk matrix domain of Martian breccia Northwest Africa 7034. *Meteorit. Planet. Sci.* **51**, 483–498 (2016).
31. Rampe, E. B. et al. Mineralogy of Vera Rubin Ridge from the Mars Science Laboratory CheMin instrument. *J. Geophys. Res.* **125**, e2019JE006306 (2020).
32. Viennet, J.-C. et al. Tardi-magmatic precipitation of Martian Fe/Mg-rich clay minerals via igneous differentiation. *Geochem. Perspect. Lett*. https://doi.org/10.7185/geochemlet.2023 (2020).
33. Filiberto, J. et al. Shergottite Northwest Africa 6963: a pyroxene-cumulate Martian gabbro. *J. Geophys. Res.* **123**, 1823–1841 (2018).
34. Leroux, H. & Cordier, P. Magmatic cristobalite and quartz in the NWA 856 Martian meteorite. *Meteorit. Planet. Sci.* **41**, 913–923 (2006).
35. Udry, A., Gazel, E. & McSween, H. Y. Jr Formation of evolved rocks at Gale Crater by crystal fractionation and implications for Mars crustal composition. *J. Geophys. Res.* **123**, 1525–1540 (2018).
36. Moyen, J.-F. The composite Archaean grey gneisses: petrological significance, and evidence for a non-unique tectonic setting for Archaean crustal growth. *Lithos* **123**, 21–36 (2011).
37. Mojzsis, S. J., Harrison, T. M. & Pidgeon, R. T. Oxygen-isotope evidence from ancient zircons for liquid water at the Earth's surface 4,300 Myr ago. *Nature* **409**, 178–181 (2001).
38. Valley, J. W. et al. 4.4 billion years of crustal maturation: oxygen isotope ratios of magmatic zircon. *Contrib. Mineral. Petrol.* **150**, 561–580 (2005).
39. Cavosie, A. J., Valley, J. W. & Wilde, S. A. in *Earth's Oldest Rocks* 2nd edn (eds Van Kranendonk, M. J. et al.) Ch. 12 (Elsevier, 2019); https://doi.org/10.1016/B978-0-444-63901-1.00012-5
40. Wilde, S. A., Valley, J. W., Peck, W. H. & Graham, C. M. Evidence from detrital zircons for the existence of continental crust and oceans on the Earth 4.4 Gyr ago. *Nature* **409**, 175–178 (2001).
41. Moyen, J.-F. & Martin, H. Forty years of TTG research. *Lithos* **148**, 312–336 (2012).
42. Blichert-Toft, J. & Albarede, F. *AGU Fall Meeting Abstracts* (AGU, 2008).
43. Drabon, N. et al. Destabilization of long-lived Hadean protocrust and the onset of pervasive hydrous melting at 3.8 Ga. *AGU Adv.* **3**, e2021AV000520 (2022).
44. Johnson, T. E. et al. An impact melt origin for Earth's oldest known evolved rocks. *Nat. Geosci.* **11**, 795–799 (2018).
45. Reimink, J. R., Chacko, T., Stern, R. A. & Heaman, L. M. Earth's earliest evolved crust generated in an Iceland-like setting. *Nat. Geosci.* **7**, 529–533 (2014).
46. Latypov, R., Chistyakova, S., Grieve, R. & Huhma, H. Evidence for igneous differentiation in Sudbury Igneous Complex and impact-driven evolution of terrestrial planet proto-crusts. *Nat. Commun.* **10**, 508 (2019).
47. Naldrett, A. J. & Hewins, R. H. in *The Geology and Ore Deposits of the Sudbury Structure* Ontario Geological Survey Special Publication Vol. 1 (eds Pye, E. G. et al.) 235–251 (Ontario Ministry of Natural Resources, 1984).
48. Grieve, R. A. F., Cintala, M. J. & Therriault, A. M. in *Processes on the Early Earth* (eds Reimold, W. U. & Gibson, R. L.) https://doi.org/10.1130/2006.2405(02) (Geological Society of America, 2006).
49. Black, B. A. & Marchi, S. Buoyant impact partial melts on ancient Mars. *J. Geophys. Res.* **129**, e2023JE008040 (2024).
50. Khan, A. et al. A geophysical perspective on the bulk composition of Mars. *J. Geophys. Res.* **123**, 575–611 (2018).

Methods

Three new polished sections, labelled SP9, SP10 and SP11, were cut and polished from a centimetric sample of NWA 7533 (MNHN, Paris).

Scanning electron microscopy

Backscattered electron (BSE) imagery and energy-dispersive spectroscopy (EDS) mapping were performed at 15 keV on the carbon-coated polished sections using various scanning electron microscopes (SEM): a Tescan VEGA II LSU SEM with an SD3 (Bruker) EDS detector (IMPMC, MNHN, Paris), a Zeiss Zigma field emission gun SEM (Laboratoire de Géologie, École Normale Supérieure, Paris) and a Zeiss Ultra 55 field emission gun SEM with two Bruker X-Flash EDS detectors (IMPMC, Sorbonne Université, Paris). Images were taken with the angle-selective backscatter detector under the following conditions depending on the sample: energy 15 or 20 kV, working distance 7.5–8.3 mm with the backscatter detector aperture 25–120 µm. EDS analyses and maps were also acquired under these conditions.

Cathodoluminescence images were taken on a ZEISS Supra 55 VP Schottky field-effect SEM with a variable-pressure chamber from the Camparis platform (Sorbonne Université, Paris). This microscope is equipped with an OPEA catholuminescence device (imaging and spectral) with a parabolic mirror. Cathodoluminescence images on quartz grains were obtained at 10 keV and a working distance of 6 mm.

Electron microprobe

All quantitative mineral analyses were made by wavelength-dispersive spectrometry at 15 keV and 10 nA on the Cameca SXFive electron microprobe equipped with LaB6 source at the Camparis analytical platform (Sorbonne Université, Paris).

Representative analyses for the quartz-bearing CLMR and for various minerals are given in Supplementary Tables 1 and 2, respectively.

Given the unique and rare nature of the sample, the least destructive analytical methods were used to obtain the composition of QBC, thus avoiding laser ablation inductively coupled plasma mass spectrometry. We opted for electron microprobe analysis paired with additional EDS mapping (Extended Data Fig. 7). The main mineral phases identified in BSE images inside the clasts were targeted with one or more microprobe analyses, depending on the grain size. The bulk QBC composition (Supplementary Table 3) was estimated from these microprobe analyses (Supplementary Table 4) and the surface area ratio of each mineral component. In some clasts, mineral grains were too small or too complex to be targeted with the microprobe (~1 µm spot). In such cases, a composition for these phases has been quantified based on EDS mapping, using the ESPRIT software from Bruker. This method prevents any structural degradation of the targeted clasts and allows exclusion of the contribution of secondary phases (calcite veins, oxides and sulfides) from the total composition.

FIB milling and TEM

Four ultrathin sections in quartz grains, about 100 nm thick, were extracted by the FIB milling technique using an FEI Strata DB 235 at IEMN, University of Lille, France. The samples were then studied by TEM with an FEI Tecnai G2-20 Twin (LaB6, 200 kV) at the Electron Microscopy Centre of the University of Lille, France. The images were taken in bright field, thus using the transmitted beam and stopping the diffracted beams with an aperture in the diffraction plane. Planar crystal defects were oriented parallel to the electron beam to determine the habit plane. Diffraction patterns were recorded by selected area electron diffraction to index the crystallographic orientation of these defects.

Raman spectroscopy

All Raman analyses were performed using a continuous-wave Raman microspectrometer Renishaw inVia Reflex for point analyses and Raman hyperspectral mapping at the grain scale to check within-sample structural heterogeneity (IMPMC, Sorbonne Université, Paris). Measurements were performed using a green 532-nm solid-state laser focused on the sample through a Leica DM2500 microscope with short-working distance 50× or 100× objectives (numerical aperture = 0.75–0.90). This configuration yields a planar resolution of approximately 1–2 µm for a laser power of less than 1 mW delivered at the sample surface, using neutral density filters to prevent irreversible thermal damage. This corresponds to a laser irradiance in the range of 0.3–1.3 10^9 Wm^{-2}. The spectral resolution for visible light is 1–1.9 cm^{-1} and the wavenumber accuracy is better than 0.5 cm^{-1}.

Secondary ion mass spectrometry

O and Si isotope analyses as well as titanium analyses were carried out in separate sessions using a CAMECA IMS 1280-HR secondary ion mass spectrometry (SIMS) instrument at the SwissSIMS (University of Lausanne). All SIMS analyses were carried out with an 8–10 µm diameter spot on the surface of polished sections. The polished sections were coated with a thin layer of gold (approximately 12 nm thick) exclusively for SIMS analysis. Isotopic analyses were performed using a Cs+ primary beam of 2 nA and charge compensated using an electron gun following routine procedures[26]. The mass resolving power was set at 2,400 to resolve molecular interferences. For both O and Si measurements, the masses of interest were detected simultaneously in multicollection mode using Faraday cups. Each analysis lasted ~3 min including 30 s of pre-sputtering of the targeted surface followed by automatic signal optimization by centring the secondary beam and 20 cycles of 5 s measurements. Repeated analyses of UNIL-Q1, QZCRWU and NL615 reference quartz[26,51] allowed correction for instrumental mass fractionation and provided an external reproducibility of 0.36‰ for $\delta^{18}O$ (2 s.d.) and 0.39–0.85‰ for $\delta^{30}Si$ (2 s.d.). $\delta^{18}O$ values are calculated relative to Vienna Standard Mean Ocean Water and $\delta^{30}Si$ relative to NBS28. All O and Si isotopic data are given in Supplementary Tables 5 and 6, respectively.

The titanium concentration of quartz was measured in another dedicated SIMS session using a O- primary beam of 3 nA focused on a 4 µm diameter spot. Masses ^{48}Ti, ^{27}Al and ^{30}Si were collected in sequence, on the axial electron multiplier, for 10 cycles. Repeated analyses of reference quartz provided an external reproducibility of 2.9% (ref. 52) and 5.6% (UNIL-Q1) for titanium concentration[53].

Every analytical spot was systematically examined under optical microscopy to ensure measurement accuracy. Spots that completely or partially missed the target were not considered.

Data availability

All data used for the figures (main, Supplementary Information and Extended Data) and the tables are available via Zenodo at https://doi.org/10.5281/zenodo.14623410 (ref. 54).

References

51. Seitz, S., Baumgartner, L. P., Bouvier, A.-S., Putlitz, B. & Vennemann, T. Quartz reference materials for oxygen isotope analysis by SIMS. *Geostand. Geoanalytical Res.* **41**, 69–75 (2017).
52. Audetat, A. et al. Characterisation of a natural quartz crystal as a reference material for microanalytical determination of Ti, Al, Li, Fe, Mn, Ga and Ge. *Geostand. Geoanalytical Res.* **39**, 171–184 (2014).
53. Seitz, S. et al. Short magmatic residence times of quartz phenocrysts in Patagonian rhyolites associated with Gondwana breakup. *Geology* **44**, 67–70 (2016).
54. Malarewicz, V. et al. Evidence for pre-Noachian granitic rocks on Mars from quartz in meteorite NWA 7533. *Zenodo* https://doi.org/10.5281/zenodo.14623410 (2025).
55. Baratoux, D. et al. Petrological constraints on the density of the Martian crust. *J. Geophys. Res.* **119**, 1707–1727 (2014).

56. Peck, W. H., Valley, J. W., Wilde, S. A. & Graham, C. M. Oxygen isotope ratios and rare earth elements in 3.3 to 4.4 Ga zircons: ion microprobe evidence for high $\delta^{18}O$ continental crust and oceans in the early Archean. *Geochim. Cosmochim. Acta* **65**, 4215–4229 (2001).
57. Valley, J. W., Bindeman, I. N. & Peck, W. H. Empirical calibration of oxygen isotope fractionation in zircon. *Geochim. Cosmochim. Acta* **67**, 3257–3266 (2003).

Acknowledgements

This research benefited from funding from the CNRS-PNP and the MNHN-ATM to B.Z. and O.B. H.L. thanks the electron microscopy facility of the Chevreul Institute, University of Lille, and funding through the CHEMACT project supported by the Ministère de l'Enseignement Supérieur de la Recherche, the region Hauts-de-France and the Métropole Européenne de Lille. The National High Magnetic Field Laboratory is supported by the National Science Foundation through NSF/DMR-2128556* and the State of Florida (MH). In Lausanne, thanks are due to T. Bovay, F. Plane and the SwissSIMS team for maintaining the instrument. In Paris, thanks are due to O. Boudouma for access to the cathodoluminescence service, and M. Fialin and N. Rividi for their help with the electron microprobe (CAMPARIS, Paris). In Lille, thanks are due to D. Troadec for his help with FIB.

Author contributions

O.B. and B.Z. conceived this study. V.M., O.B., B.Z., D.D., S.P. and R.H.H. acquired the petrological and mineralogical data (SEM, Raman, electron microprobe). J.M.-C., D.R., A.S.B. and E.B. acquired the SIMS data. H.L. acquired the TEM data. All authors were involved in the interpretation of the data. O.B. led the writing of the paper to which all co-authors contributed with comments and inputs.

Competing interests

The authors declare no competing interests.

Additional information

Extended data is available for this paper at https://doi.org/10.1038/s41561-025-01653-z.

Supplementary information The online version contains supplementary material available at https://doi.org/10.1038/s41561-025-01653-z.

Correspondence and requests for materials should be addressed to O. Beyssac.

Peer review information *Nature Geoscience* thanks Alan Hastie, Michael Phillips and the other, anonymous, reviewer(s) for their contribution to the peer review of this work. Primary Handling Editor: Alison Hunt, in collaboration with the *Nature Geoscience* team.

https://doi.org/10.1038/s41561-025-01653-z

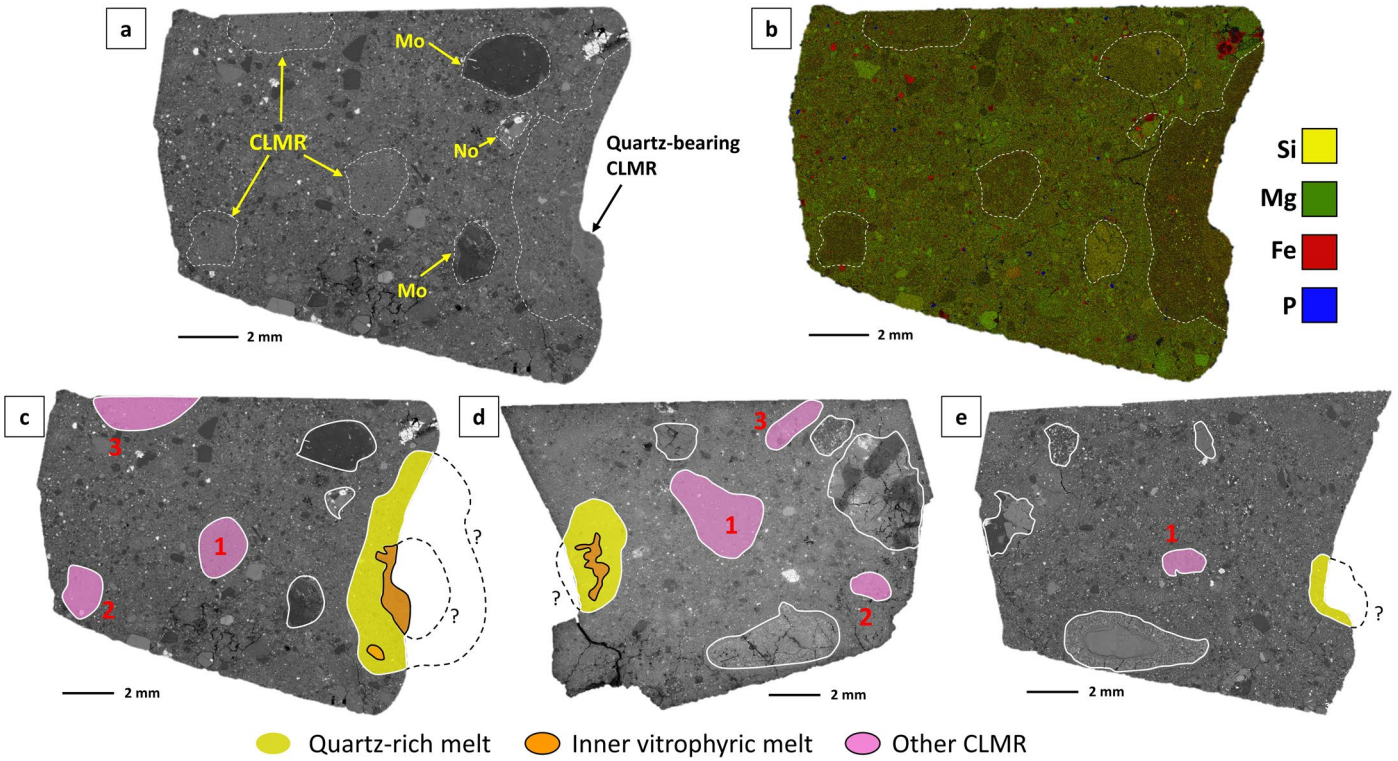

Extended Data Fig. 1 | Variability and location of CLMR in several sections of NWA 7533. (**a**) SEM image in BSE mode of the NWA 7533 section (SP10) with its different components: CLMR (Clast Laden Melt Rock), Mo (monzonitic clast), No (Noritic clast) and quartz-bearing CLMR. (**b**) SEM EDS mapping of the NWA 7533 section (SP10) with Si, Mg, Fe and P represented. All quartz fragments are located within a distinct Mg-poor and Ca-rich quartz-bearing CLMR in the right part of the section. This quartz-bearing CLMR (highlighted in yellow in C, D and E), including its inner vitrophyric melt (in orange) can be traced through 3 distinct polished sections in the same piece of NWA 7533: SP10 (**c**), SP9 (**d**) and SP11 (**e**). Extrapolating the shape of this zone at the edge of each section suggests a roundish shape with a vitrophyric core. Several CLMR (in pink numbered from 1 to 3) and some prominent lithic clasts (circled in white) can be traced through the sections, highlighting the spatial continuity.

https://doi.org/10.1038/s41561-025-01653-z

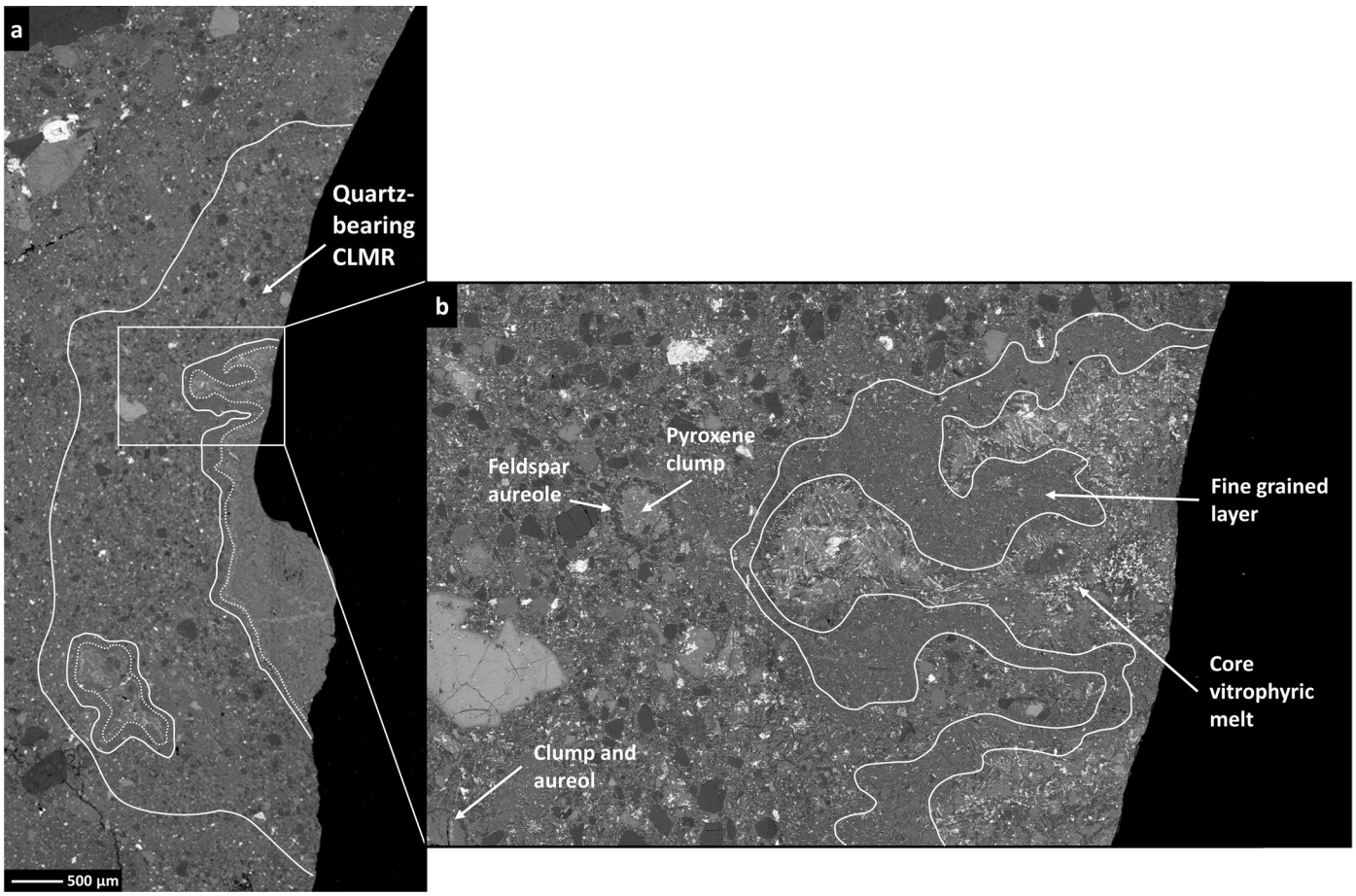

Extended Data Fig. 2 | Petrology of the quartz-bearing CLMR. (**a**) SEM BSE map of the quartz-bearing CLMR where all the quartz grains, including those contained in quartz-bearing clasts, were found in section SP10. (B) The close-up BSE map illustrates the varied and complex microtextures observed in this melt zone, including pyroxene clumps with a plagioclase aureole as described in Hewins et al.[8]. A fine-grained rim surrounds the inner vitrophyric melt (**b**).

https://doi.org/10.1038/s41561-025-01653-z

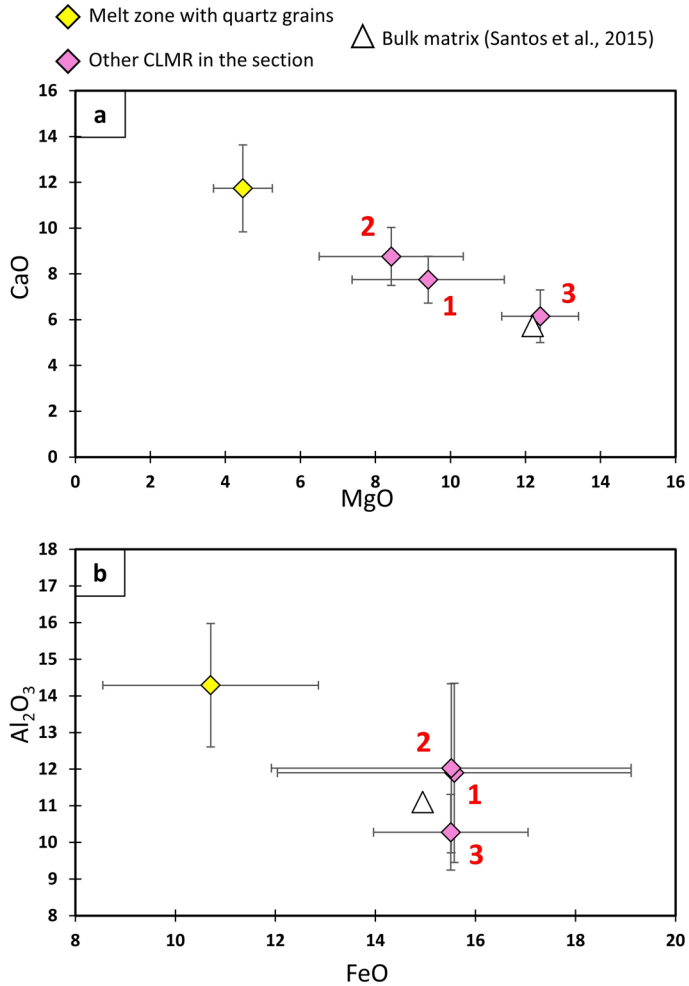

Extended Data Fig. 3 | Chemical composition of CLMR in NWA 7533. Chemical composition of the quartz-bearing CLMR (in yellow) and of other CLMR (in pink, see Extended Data Fig. 2 for location of each CLMR from corresponding numbers) compared to the bulk matrix of NWA 7533[7]. (**a**) CaO versus MgO, (**b**) Al_2O_3 versus FeO. Average compositions are derived from the average of electron microprobe data obtained on a series of ten to twenty 12*9 µm raster point analyses. Error bars are standard deviations for these analyses (see Supplementary Table 1).

https://doi.org/10.1038/s41561-025-01653-z

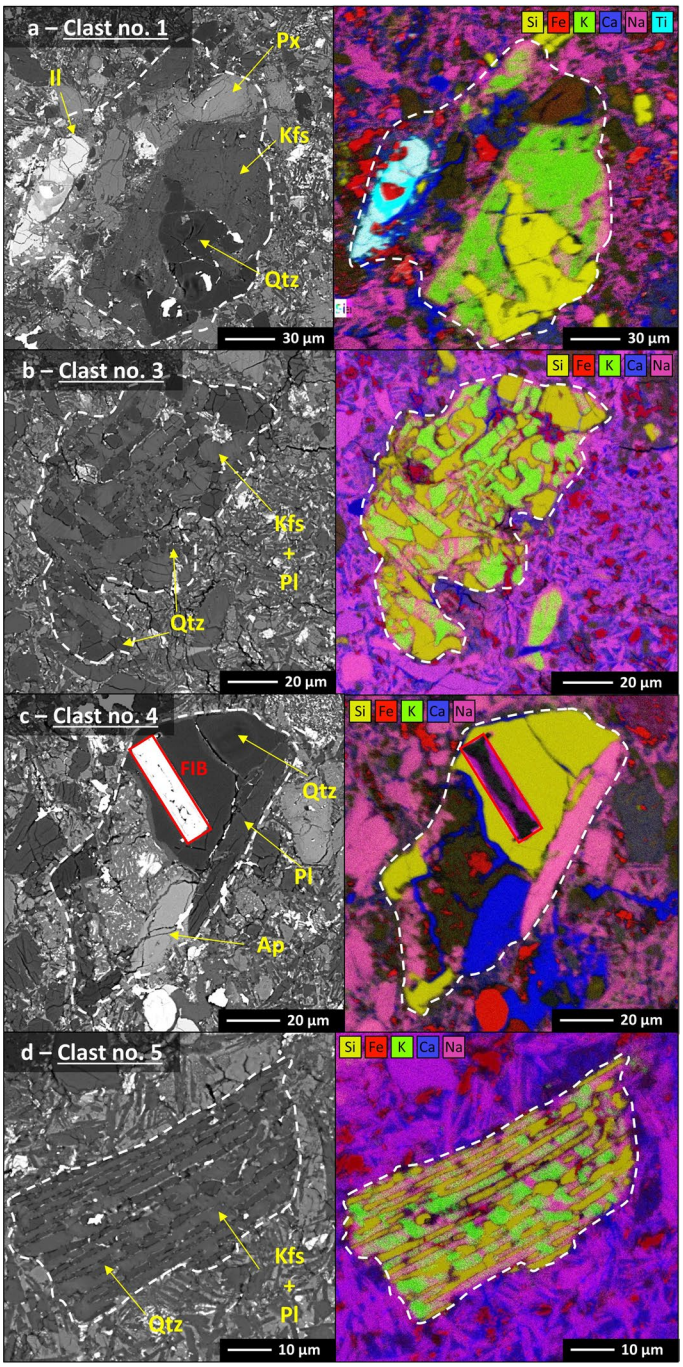

Extended Data Fig. 4 | Petrology and chemical composition of quartz-bearing clasts. SEM BSE images and corresponding SEM EDS mapping of four quartz-bearing clasts (QBC) identified in the quartz-bearing CLMR of NWA 7533. The lithic clasts shown are (**a**) clastno. 1, (**b**) clast no. 3, (**c**) clast no. 4, and (**d**) clast no. 5. Qtz = quartz, Kfs = K-feldspar, Pl = plagioclase, Px = pyroxene, Il = ilmenite, Ap = apatite.

https://doi.org/10.1038/s41561-025-01653-z

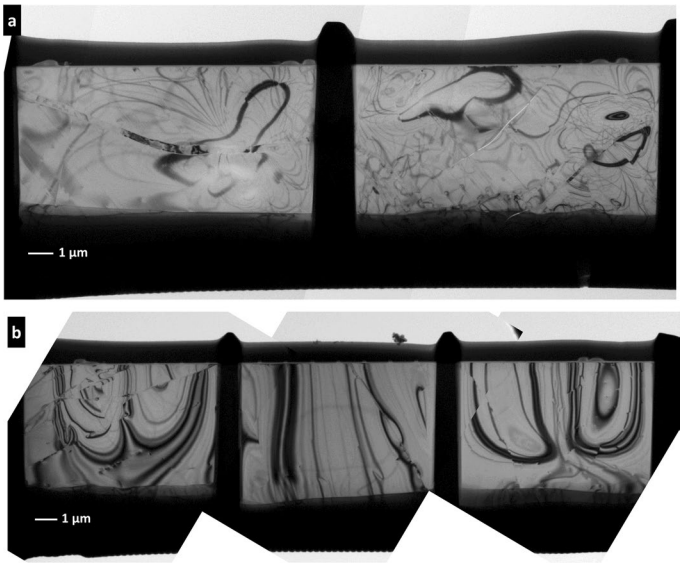

Extended Data Fig. 5 | TEM imaging of FIB sections in quartz. Mosaic of TEM images in low magnification bright-field mode of two FIB sections from Qtz no. 13 (**a**) and Qtz no. 10 (**b**). In both cases, quartz appears as single crystal with only minor defects. Bragg fringes are disrupted by planar defects interpreted as shock features at low intensity.

https://doi.org/10.1038/s41561-025-01653-z

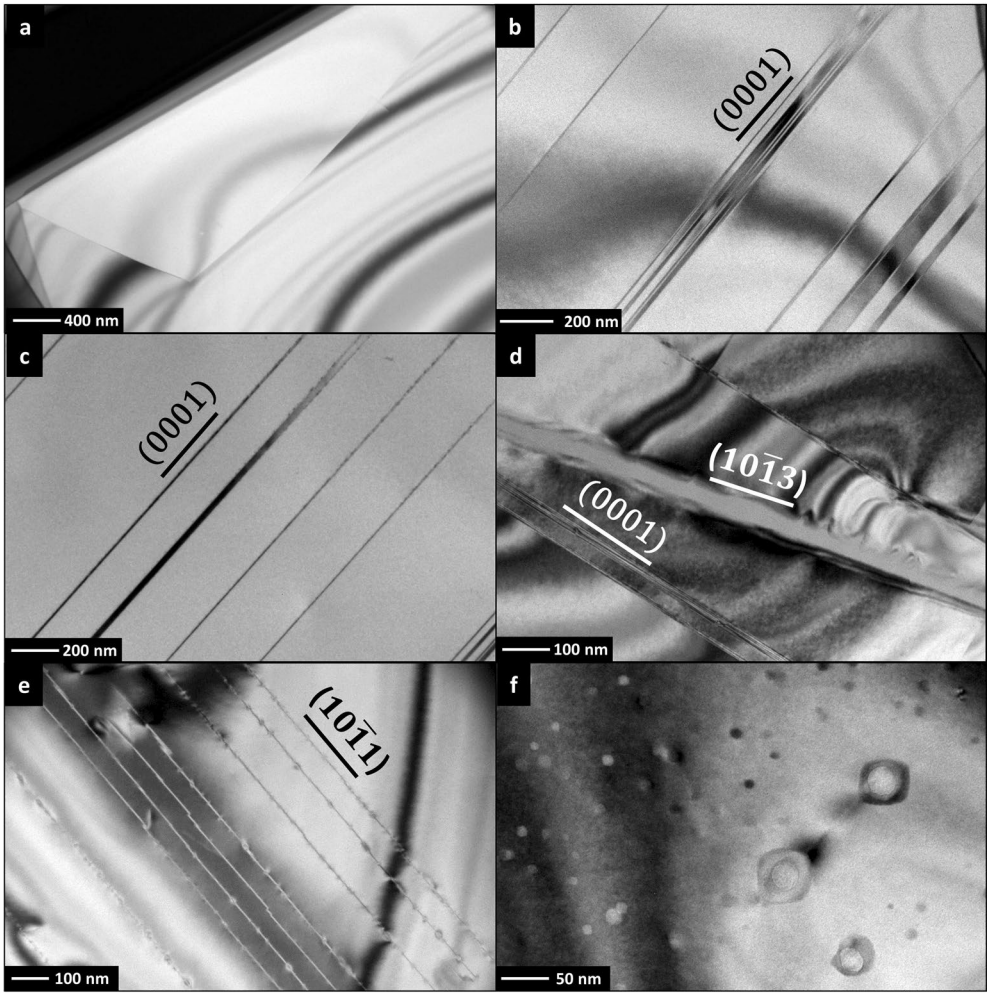

Extended Data Fig. 6 | High-resolution images within the FIB sections obtained by TEM in bright field mode. (**a**) Growth twins at the edge of the section from Qtz no. 10. Mechanical twinning in (0001) in Qtz no. 13 (**b**,**c**). (**d**) Lamellae of amorphous material in (10$\bar{1}$3) together with mechanical twins within Qtz no. 10. (**e**) Beam of planar defects in (10$\bar{1}$1) within the Qtz no. 2. (**f**) Small mineral inclusions linked by a thin planar defect within Qtz no. 13.

https://doi.org/10.1038/s41561-025-01653-z

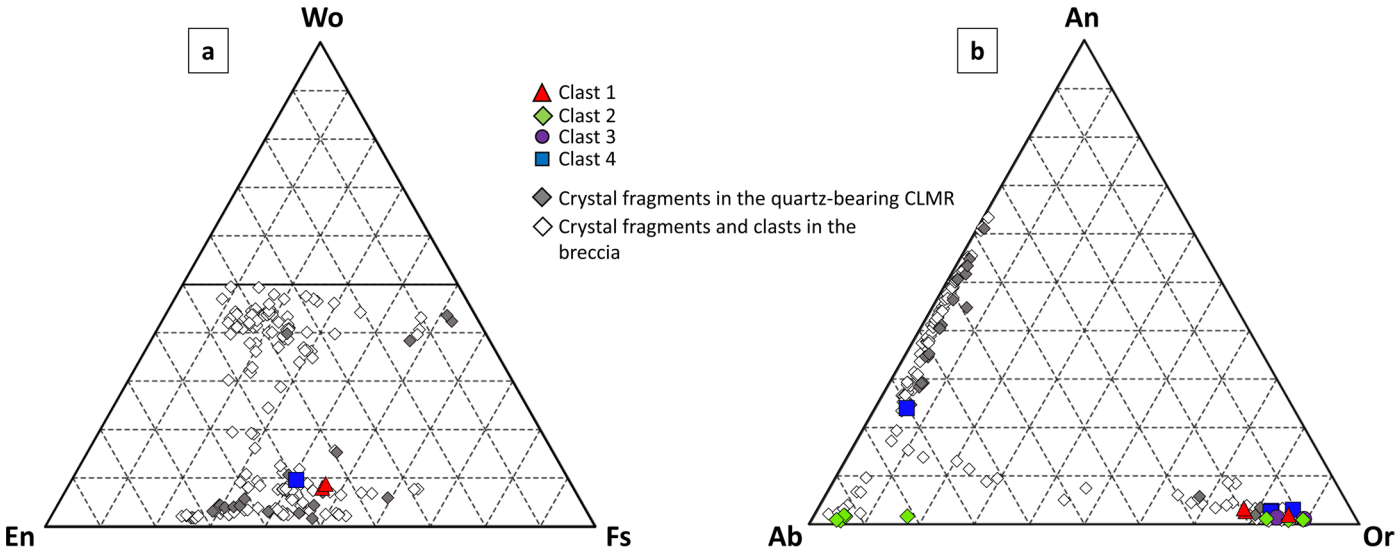

Extended Data Fig. 7 | Mineral composition in quartz-bearing clasts. Composition of pyroxene (**a**) and feldspar (**b**) in quartz-bearing clasts (clasts 1 to 4) and other individual fragments found in the quartz-bearing CLMR and in the matrix of the breccia[8]. Compositions were analysed by electron microprobe. Mineral phases in clast #5 are too small to be analysed by electron microprobe.

https://doi.org/10.1038/s41561-025-01653-z

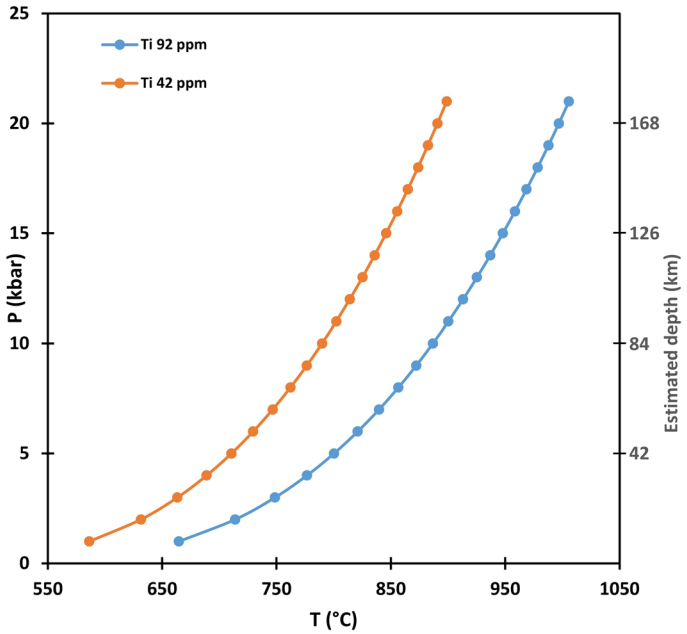

Extended Data Fig. 8 | Crystallization conditions for quartz from Ti-in-quartz thermometry. Ti-in-quartz calibration curves in a pressure-temperature diagram[28] for the two Ti concentrations measured in this study. A simple depth scale is given as a comparison, calculated assuming a density of 3200 kg.m^{-3} within the upper Martian crust[55].

https://doi.org/10.1038/s41561-025-01653-z

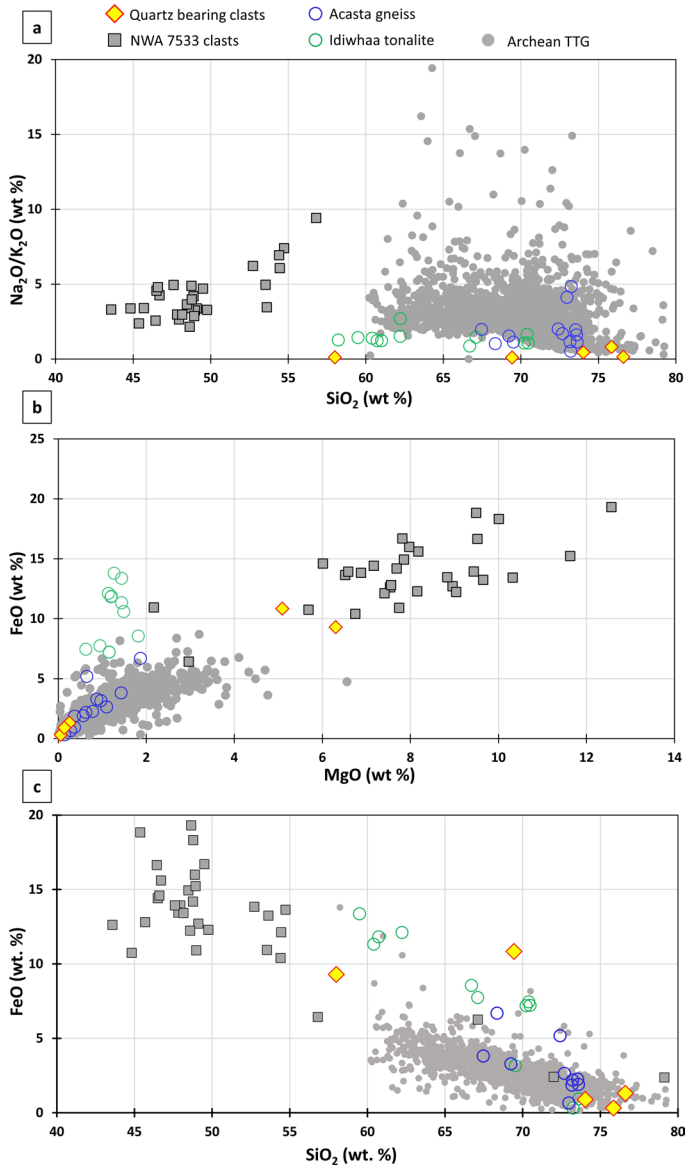

Extended Data Fig. 9 | Geochemistry of quartz-bearing clasts. Geochemical diagrams comparing the composition of the quartz-bearing clasts with other lithic clasts in the NWA 7533 (and paired meteorites) breccia[6–8], and terrestrial rocks like the Archean TTGs[36], the Acasta gneiss and Idiwhaa tonalite[44]. (**a**) Na_2O/K_2O versus SiO_2, (**b**) FeO versus MgO, (**c**) FeO versus SiO_2.

https://doi.org/10.1038/s41561-025-01653-z

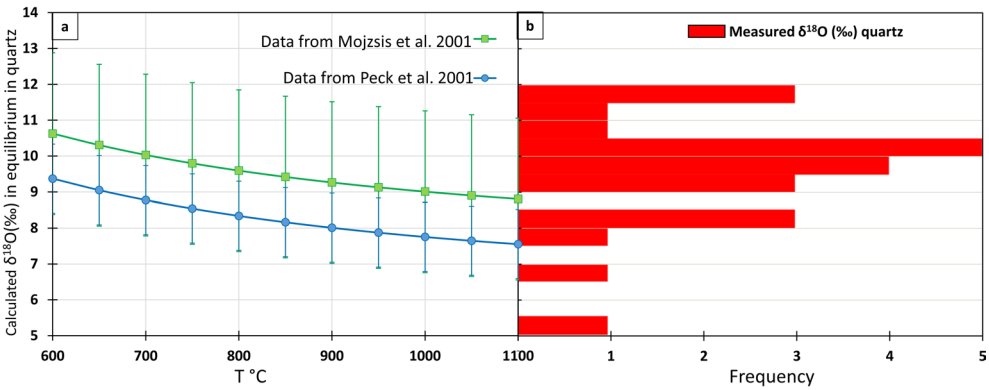

Extended Data Fig. 10 | Isotopic comparison with Jack Hills zircons. (**a**) Calculation of $\delta^{18}O$ for quartz in equilibrium with zircon versus temperature for the Hadean Jack Hills zircons. Zircon $\delta^{18}O$ data are from 6 zircons in Peck et al.[56] and 18 zircons in Mojzsis et al.[37], and the oxygen fractionation is taken from Valley et al.[57]. Each point is the average of calculated values and the error is their standard deviation. (**b**) The $\delta^{18}O$ values measured in the Martian quartz are shown in the histogram plot for comparison.